# Seismic deformation pattern in the Friuli-Venezia Giulia region (north-eastern Italy) and western Slovenia

G. Bressan and P.L. Bragato

*Dip. Centro di Ricerche Sismologiche, Ist. Naz. di Oceanografia e di Geofisica Sperimentale, Udine, Italy*

(Received: November 26, 2007; accepted: June 25, 2008)

***ABSTRACT*** Ten deforming belts of relatively homogeneous deformation have been recognized in the Friuli-Venezia Giulia region (north-eastern Italy) and in western Slovenia, by comparing tectonic and seismological characteristics. The seismic deformation rates of each belt have been calculated from moment tensor summation for the period 1984-2006. The results indicate that the deformation pattern is heterogeneous with a significant strain partitioning among the deforming belts. The belts located in the western part of the study area are undergoing a compressional strain that is changing orientation from a NW-SE to a NNW-SSE direction. The prevailing mode of deformation of the northern and eastern belts in this part of the study area is related to a dextral strike-slip motion, along directions switching from NNE-SSW to NW-SE. The deformation geometry of the belts located in the central part of the study area is mainly compressional, N-S oriented. The rates of deformation of the belts related to the dominant mode of deformation vary from 4.8 x $10^{-5}$ mm/year to 0.24 mm/year.

## 1. Introduction

The present paper focusses on the investigation of the seismic deformation pattern of the Friuli-Venezia Giulia Region and western Slovenia. The study area is divided into seismogenic sources of relatively homogeneous deformation (deforming belts). Their identification is mainly performed on the basis of the seismicity pattern, tectonic structures and the type of focal mechanisms. The purpose is to determine the geometry of seismic deformation and the deformation rates of each belt from the moment tensor summation method. The period examined is from 1984 to 2006.

We estimate the moment tensor components from the focal mechanism solutions computed with P-wave polarities. The moment tensor summation is a suitable technique (Kostrov, 1974; Jackson and McKenzie, 1998) for providing a quantitative analysis of seismic strain, the dominating tectonic processes and their role in the seismotectonics of a region. The method is helpful in reconstructing the kinematics of present day crustal motion. Furthermore, the percentage of deformation accommodated aseismically can be evaluated from the comparison between geodetic strain measurements and seismic strain. This aspect also play a significant role in the evaluation of seismic hazard.

The moment tensor summation method was applied by Pondrelli *et al.* (1995) and Pondrelli

 

(1999) to investigate the strain pattern of the Mediterranean area. The deforming area of the Eastern Alps including the Veneto region, the Friuli-Venezia Giulia region and the western Slovenia was modelled by Pondrelli (1999) as a straight box.

## 2. Tectonic framework

The Friuli-Venezia Giulia region (north-eastern Italy) and the western Slovenian area are part of a polyphase deformational zone located in the northern margin of the Adria microplate. The complex tectonic setting (Fig. 1) was produced from the Eocene to the Plio-Quaternary by the progressive convergence of the Adria microplate and its anticlockwise rotation with respect to the Eurasian plate (Anderson and Jackson, 1987; Ward, 1994; Nocquet and Calais, 2003; Grenerczy *et al.*, 2005). The motion was accommodated by complex mechanisms of crustal shortening and indentation (Mantovani *et al.*, 1996) against the eastern Southern Alps and was characterized by the superimposition of several Cenozoic tectonic phases (Castellarin *et al.*, 1992).

The tectonic setting appears to be characterized (Venturini, 1991; Bressan *et al.*, 2003) by two indented structural wedges (Fig. 1), denoted the outer and the inner, outlined by NE-SW and NW-SE paleofault systems. According to Venturini (1991), several syn-sedimentary tectonic movements, active from the late Carboniferous to the middle Miocene, produced extensional fault systems NE-SW oriented (PC-VB and TV-BC lineaments, Fig. 1) and NW-SE oriented (ML and D-I lineaments, Fig. 1), forming the indented wedges. Later, the compressive Cenozoic tectonic phases re-activated the early syn-sedimentary faults, producing a peculiar tectonic pattern. The Mesoalpine (Dinaric) NE-SW earliest compression generated NW-SE-oriented thrusts that affected mainly the Slovenian and the central and southern part of the Friuli area. From the middle Miocene to the earliest Pliocene, the N-S trending Alpine compression produced E-W oriented systems of south-verging thrusts and backthrusts, with severe shortening of the upper crust in the central part of the area. Castellarin (1979) estimated that its original extent was reduced to about one third. The early syn-sedimentary faults were re-activated as strike-slip faults. During Pliocene times, a NW-SE-oriented compression produced mainly NE-SW trending thrusts and folds. This tectonic phase mainly affected the north-western part of the area, where the WSW-ENE and the E-W trending thrusts and backthrusts generated by the Alpine compression phase were re-activated as dextral strike-slip faults.

Each phase inherited and re-activated the geological deformations of the previous phase producing a complex deformation pattern. As a consequence, the crustal structure appears very fragmented, as shown by deep seismic sounding (DSS) profiles (Scarascia and Cassinis, 1997), with segmentation of the main shallow tectonic lineaments (Slejko *et al.*, 1989; Galadini *et al.*, 2005).

This complex tectonic-structural setting of the Friuli area was put in evidence also by the 3-D Vp and Vp/Vs tomographic images of the Friuli area (Gentile *et al.*, 2000). The upper crust is characterized by discontinuous blocks and wedges, marked by lateral heterogeneities in Vp and Vp/Vs values, interpreted as variations of the mechanical strength of the rocks. The structural heterogeneity of the crust has been revealed also by the spatial complex pattern characterizing the shear modulus, the Poisson ratio and the bulk modulus (De Franco *et al.*, 2004).

Slejko *et al.* (1989) proposed a seismotectonic model whose kinematics and tectonic patterns

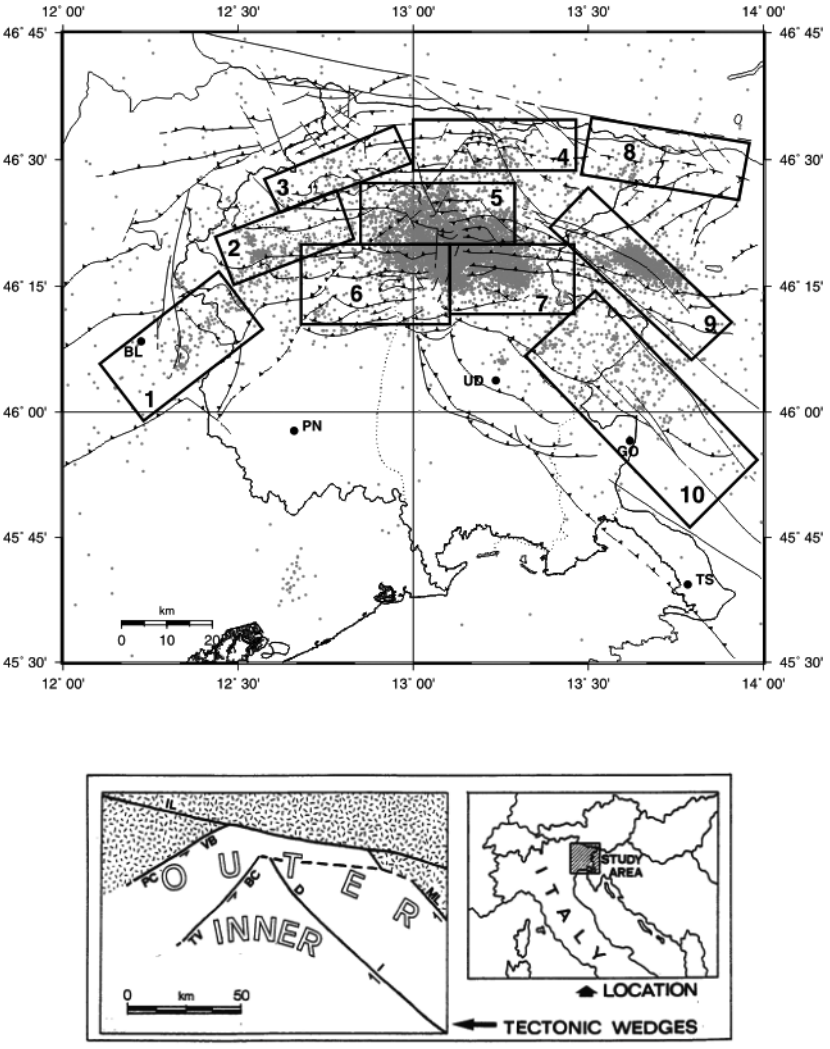


Fig.1 - Tectonic pattern of the north-eastern Italy and western Slovenia; solid and dashed lines: subvertical faults, barbed lines: thrust. The main deforming belts, numbered 1-10, are also shown. Gray dots represent the earthquakes with $M_D$ ranging from 1.0 to 5.6, recorded by the OGS local seismic network from 1977 to 2006, with vertical and horizontal errors less than, or equal to, 3 km. The inset shows the two indented tectonic wedges as depicted by the paleofaults re-activated during the Mesoalpine and Alpine tectonic phases. PC-VB: Pieve di Cadore - Val Bordaglia line; TV-BC: Tramonti - But-Chiarsò line; D-I: Dogna - Idria line; IL: eastern Insubric lineament (Gailtal line); ML: Mojstrana - Ljubljana line. BL: Belluno; PN: Pordenone; UD: Udine; GO: Gorizia; TS: Trieste (modified from Bressan *et al.*, 2003; Vai *et al.*, 2002; Poli *et al.*, 2002).

are similar to that by Venturini (1991), although the paleofault TV-BC (Fig. 1) was not recognized. In such a model, the structure of the upper crust consists of a sedimentary cover of mainly mesozoic and Paleozoic units, deformed by a mechanism of imbrication and shortening that generated more or less E-W oriented thrusts. The crustal shortening is accommodated also by north-vergent backthrusts. The geological cross-sections of Carulli and Ponton (1992), Merlini

*et al.* (2002) and Poli *et al.* (2002) follow this structural interpretation. The Paleozoic basement is detached from the overlying sedimentary cover and was partly involved in thrusting. The Dinaric lineaments (NW-SE oriented faults and buried thrusts under the plain) mainly affect the eastern part of the study area. The upper crustal structure of the Friuli area is characterized by a complex deformation pattern with fragmentation and incorporation of the Dinaric structures in the southalpine ones (Carulli and Ponton, 1992). According to Slejko *et al.* (1989), the neotectonic activity from middle Pleistocene to Holocene times mainly affected the central sector of the area (Slejko *et al.*, 1989), with uplifting and tilting of the southernmost thrust belts. The recent study by Galadini *et al.* (2005) confirms this trend.

The present-day seismic activity (Fig. 1), recorded from 1977 by the local short-period seismic network of the Istituto Nazionale di Oceanografia e di Geofisica Sperimentale (OGS), mainly affects the central part of the Friuli-Venezia Giulia region with localized clusters in the northern and western parts of the area and western Slovenia. The seismotectonic characteristics are heterogeneous. The fault plane solutions are mainly of thrust type, even if with different nodal plane orientations, with a significant number of strike-slip and minor normal faulting events (Gentile and Slejko, 1990; Bressan *et al.*, 2003; Poli and Renner, 2004). Several distinct seismotectonic domains have been recognized and the present stress field is characterized by different stress patterns, with variations in principal stress orientation and stress regime (Bressan *et al.*, 2003).

The seismicity pattern, the various types of focal mechanisms and the different tectonic domains suggest that the complex tectonic interaction and indentation of the Adria microplate and Eurasian Plate in the Friuli-Venezia Giulia region and in western Slovenia are accommodated by several deformation belts.

## 3. Data

Since 1977 the seismicity of the region has been recorded by the short-period local seismic network operated by the OGS. The initial configuration of seven analog stations was implemented in 1984 with 16 seismometers that represent the present permanent short-period network geometry. Since 1988 the network has been updated by digital acquisition.

The seismic events were located with the HYPO71 program (Lee and Lahr, 1975). The crustal model used for the earthquake location consists of two layers and a half-space (depth 0-22 km with Vp=5.85 km/s; depth 22-39.5 km with Vp=6.8 km/s; depth > 39.5 km with Vp=8.0 km/s; Vp/Vs=1.78). The seismicity that occurred in western Slovenia mainly consists of events of the 1998 and 2004 Bovec sequences, located also with the arrival times of permanent and temporary stations, provided by Bajc *et al.* (2001) and by Zivcic (personal communication). Six temporary portable short-period stations of the OGS network have also been used since 2002.

The HYPO71 locations in the Friuli-Venezia Giulia region were compared with the relocations obtained from the 3-D Vp-Vs tomographic model of Gentile *et al.* (2000). The average differences in latitude and longitude are of about 1 km and the depth location varies from 1 to 2 km (Bressan *et al.*, 2003). Similar differences (Bressan *et al.*, 2007) are found in the Slovenian 1998 sequence (mainshock $M_D$ 5.6) with the locations of Bajc *et al.* (2001). The values of magnitude are given in duration magnitude $M_D$, computed according to Rebez and Renner

Table 1 - Type of focal mechanisms of the deforming belts according to the classification of Zoback (1992): NF=normal faulting, NS=predominant normal faulting with strike-slip component, SS=strike-slip faulting, TS=predominant thrust faulting with strike-slip component, TF= thrust faulting, U=unknown.

| Belt | Number | NF | NS | SS | TS | TF | U |
|---|---|---|---|---|---|---|---|
| 1 | 20 | 1 | | 6 | | 11 | 2 |
| 2 | 36 | 6 | 2 | 5 | 1 | 19 | 3 |
| 3 | 21 | 6 | 3 | 6 | | 5 | 1 |
| 4 | 10 | 6 | | 3 | | 1 | |
| 5 | 64 | 3 | 1 | 13 | 7 | 34 | 6 |
| 6 | 22 | 5 | | 4 | | 12 | 1 |
| 7 | 26 | 2 | | 3 | 4 | 15 | 2 |
| 8 | 14 | 4 | | 2 | 1 | 6 | 1 |
| 9 | 44 | 4 | 5 | 16 | 5 | 13 | 1 |
| 10 | 22 | 3 | 2 | 2 | 2 | 7 | 6 |
| Tot | 279 | 40 | 13 | 60 | 20 | 123 | 23 |

(1991).

In order to apply the moment tensor summation method, the focal mechanism of 279 earthquakes with magnitude $M_D$ ranging from 1.5 to 5.6 were considered. They were computed using the P-wave first motion (Whitcomb,1973), using also polarity data from seismic stations outside the Friuli-Venezia Giulia region from the bulletin of the International Seismological Centre. The procedure of Whitcomb (1973) elaborates the focal mechanism that minimizes the number of first motion polarities in error, by testing a grid of trial mechanisms with a resolution of 5°. A linear function tapers the polarities from zero to unity within a distance of 3° from the nodal plane. The number of focal mechanisms for each deforming belt and their classification according to Zoback (1992) are summarized in Table 1.

## 4. Method

The method of analysis is based on the formulation of Kostrov (1974) and Jackson and McKenzie (1988). Following Kostrov (1974), the average strain rate tensor $\dot{\varepsilon}$ of a seismic zone is related to the sum of the earthquake moment tensors by:

$$\dot{\varepsilon}_{ij} = \frac{1}{2\mu V \tau} \sum_{k=1}^{K} M_{ij}^{k} \qquad (1)$$

where $\mu$ is the shear modulus of the crustal rocks, $V$ the deformed volume, $M_{ij}^{k}$ is the $ij$th component of the moment tensor $M$ of the $k$th event, $\sum_{k=1}^{K} M_{ij}^{k}$ is the sum of the moment tensors of the earthquakes that occurred within the volume in $\tau$ years.

The volume $V$ considered is a rectangular box with sides $l$ (length), $a$ (width) and $t$ (thickness or depth extent of the seismogenic layer). The components of the velocity tensor of motion, in a reference system where $x$ is normal, $y$ is parallel and $z$ is vertical with respect to the average trend of the deforming belt, or the strike of the side $l$, are calculated with the following relations:

$$V_X^X = \frac{1}{2\mu lt\tau}\sum_{n=1}^{N} M_{11}^n \tag{2}$$

$$V_Y^Y = \frac{1}{2\mu at\tau}\sum_{n=1}^{N} M_{22}^n \tag{3}$$

$$V_Z^Z = \frac{1}{2\mu al\tau}\sum_{n=1}^{N} M_{33}^n \tag{4}$$

$$V_Y^X = \frac{1}{\mu lt\tau}\sum_{n=1}^{N} M_{12}^n \tag{5}$$

$$V_Z^X = \frac{1}{\mu al\tau}\sum_{n=1}^{N} M_{13}^n \tag{6}$$

$$V_Z^Y = \frac{1}{\mu al\tau}\sum_{n=1}^{N} M_{23}^n. \tag{7}$$

$V_X^X$ represents the component of motion, normal to the side $l$, $V_Y^Y$ is the sideways expulsion of material, normal to side $a$ and $V_Z^Z$ is the thickening rate (Pondrelli *et al.*, 1995).

Jackson and McKenzie (1988) pointed out that the off-diagonal components of the moment tensor do not have a simple physical interpretation. However, with the condition that the length $l$ of the deforming box is much greater than its width $a$, the horizontal shear velocity $V_Y^X$ corresponds to the amount of strike-slip motion. The other off-diagonal components are not considered in the present analysis.

Sign conventions are as follows (Pondrelli *et al.*, 1995). Positive values of the components perpendicular to the box faces represent extension or thickening and negative values represent compression or thinning. The strike-slip component $xy$ is positive for dextral motion and negative for sinistral motion. The seismic moment tensors are rotated in the local coordinate system (length/width/depth) as defined in Eqs. (1) – (7). The value of shear modulus is assumed $3.0 \cdot 10^{-4}$ MPa. The seismic moment in N·m is obtained from duration magnitude with the relation (Franceschina *et al.*, 2006):

$$\log M_0 = 1.46 M_D + 8.83 \qquad \sigma_{\log M_0} = \pm 0.30. \tag{8}$$

As shown by Papazachos and Kiratzi (1992), the errors in the magnitude of the strain and velocity rates, are controlled by errors in the scalar annual moment rate. We found that the uncertainties, calculated following the approach of Wyss *et al.* (1992), affect the deformation rates by about a factor 2.

## 5. Deforming belts

The study area has been divided into 10 rectangular deforming belts (Figs. 1 and 2) of relatively homogeneous deformation in order to analyze the spatial pattern of the strain rate tensor.

Each belt includes the main tectonic lineaments and the major earthquakes that occurred during the examined period, from 1984 to 2006. Where available, geophysical data as tomographic images (Gentile *et al.*, 2000) and Bouguer anomaly patterns (Cassano *et al.*, 1989) were also used. The belts were recognized on the basis of the seismicity pattern, seismic activity and similarity of focal mechanisms. Fig. 2 also shows the location of major historical earthquakes

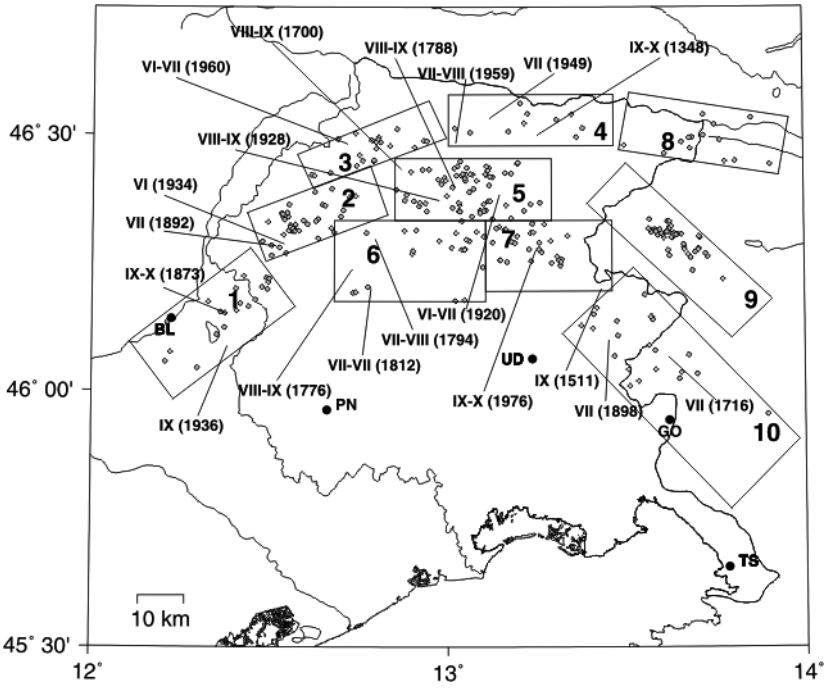


Fig. 2 - Deforming belts and location map of the earthquakes (dots) used in the strain rate tensor computation. The location of the strongest historical earthquakes, with the epicentral intensity and the year of occurrence in parentheses, is also shown. Other symbols as in Fig. 1.

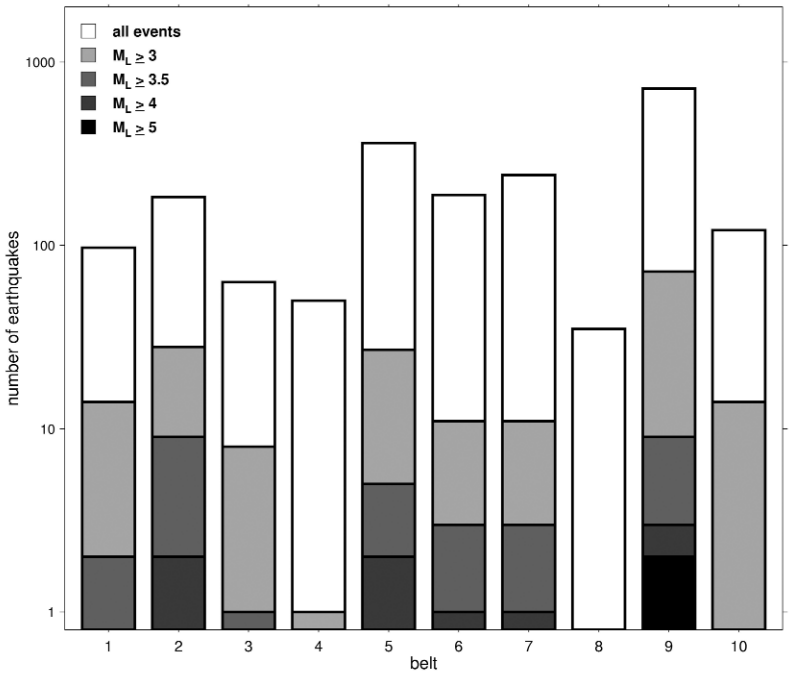


Fig. 3 - Number of earthquakes with respect to the duration magnitude of each deforming belt.

(Barbano, 1990, 1993; Barbano *et al.*, 1985; Camassi and Stucchi, 1997; CPTI Working Group, 2004). Historical earthquakes were reported only as additional information and they were not considered as a definition of the deforming belts because of the uncertainties about the historical data. However, the location of most of them appears consistent with the recognized deforming zones. The seismic activity of each deforming belt is summarized in Fig. 3 and the distribution of the cumulative radiated seismic energy with depth is shown in Fig. 4. The earthquakes have been selected with vertical and horizontal location errors of less than, or equal to, 3 km and with magnitude threshold $M_D$ 2.0.

The radiated seismic energy is calculated using the relation between the seismic energy and the duration magnitude of Franceschina *et al.* (2006):

$$\log E = 1.94 M_D + 2.26 \qquad \sigma_{\log E} = 0.52. \tag{9}$$

The focal mechanisms resulting from the cumulative moment tensors of each deforming belt are shown in Fig. 5.

### *5.1. Belt 1*

The tectonic pattern is characterized by thrusts with different orientations and high-angle dipping faults, with a N-S trend. The seismic activity detected in the considered period is low

with respect to the other deforming belts (Fig. 3). The maximum recorded magnitude was 3.6. Most of the radiated seismic energy is located between a depth of 8 and 11 km (Fig. 4). The seismogenic layer extends down to a 17 km depth. Most of the focal mechanism shows reverse faulting (Table 1). Strike-slip events are also present.

Despite the present low seismic activity, this zone experienced severe earthquakes in the past (Fig. 2): the 1873 event with epicentral intensity $I_0$ = IX-X MCS on the Mercalli-Cancani-Sieberg scale (estimated magnitude 6.3) and the 1936 event with $I_0$ = IX (estimated magnitude 5.9). Sirovich and Pettenati (2004) elaborated the focal mechanism of the 1936 event by inverting its regional macroseismic intensity pattern. The focal mechanism is inverse with the rupture plane NE-SW oriented and NW-SE 47° dipping.

### *5.2. Belt 2*

The main tectonic lineaments are south-verging thrusts with N80°-90°E trending planes, dipping at 40° to 60° to the north. The thrust system is rotated in the western part, assuming a NW-SE orientation. According to Bernardis *et al.* (1996), the deforming zone is affected by upper crustal shortening, NNW-SSE oriented, accommodated by WSW-ENE striking inverse faults. The seismic activity is low to moderate (Fig. 3), with radiated seismic energy mostly distributed between a 9 and 14 km depth (Fig. 4). The thickness of the seismogenic layer is 20 km. The most relevant seismic sequences that occurred in the examined period were triggered by the following mainshocks: the $M_D$ 4.1 event occurred on August 29, 1986, the $M_D$ 3.7 event occurred on April 20, 1994 and the 1996 swarm, with 3 main episodes occurred on January 27 ($M_D$ 3.5), on February 27 ($M_D$ 3.8) and on April 13 ($M_D$ 4.3). The predominant fault plane solutions are of thrust type (Table 1) The belt is characterized also by normal and strike-slip events. The best documented historical events occurred in 1892 with $I_0$ = VII and 1934 ($I_0$ = VI), with estimated magnitudes 4.8 and 4.7, respectively (Fig. 2).

### *5.3. Belt 3*

The main tectonic lineaments are WSW-ENE trending and SSE-verging thrusts and folds. According to Venturini (1991), these tectonic structures underwent dextral strike-slip displacement after the Pliocene NW-SE trending compression. The seismic activity is low (Fig. 3), with most of the radiated seismic energy located between an 8 and 11 km depth (Fig. 4). The thickness of the seismogenic layer is about 14 km. The maximum recorded magnitude was 3.7 (June 19, 1999). No relevant seismic sequences were detected. The belt is characterized by heterogeneous fault plane solutions (Table 1). The available historical data does not point to strong earthquakes in the past. The best documented event occurred in 1960 (Fig. 2) and was characterized by $I_0$ = VI-VII (estimated magnitude 4.3).

### *5.4. Belt 4*

This deforming zone includes the apical part of the inner wedge (Fig. 1) outlined by the NE-SW and NW-SE oriented paleofaults. This belt is characterized also by E-W oriented, south-verging thrusts and the E-W oriented Fella-Sava backthrust, that is the most extended tectonic lineament. The Fella-Sava Line, according to the kinematic model of Venturini (1991), was forced into a dextral strike-slip motion owing to the Pliocene NW-SE trending compression. Merlini *et al.* (2002) recognized the Fella-Sava Line as a vertical fault with dextral transpressive component.

NW-SE right-lateral faults are also present. The seismic activity detected in the considered period is low (Fig. 3), with maximum recorded duration magnitude 3.4. The cumulative radiated seismic energy (Fig. 4) puts in evidence a maximum at a depth of about 8 km. The seismogenic layer extends down to about 17 km depth. Few focal mechanisms are available (Table 1), mainly normal and strike-slip solutions. In this belt, the most severe earthquake that struck the Friuli-Venezia Giulia region ($I_0$ = IX-X, estimated magnitude 6.7) seems to have occurred (Fig. 2) in 1348. However, the location of this earthquake is still under debate because of the uncertainties about the historical data (Camassi and Stucchi, 1997; CPTI Working Group, 2004). The best documented major earthquakes were the 1949 event with $I_0$ = VII (estimated magnitude 4.8) and the 1959 event with $I_0$ = VII-VIII (estimated magnitude 4.9).

### *5.5. Belt 5*

The tectonic pattern consists mainly of E-W thrusts and backthrusts. Vertical fault systems, bending N140°-150°E and N20°-30°E intersect the reverse faults. According to Venturini and Carulli (2002), this area experienced the strongest Alpine compression and crustal shortening during Miocene times. The recorded seismic activity appears moderate-to-high (Fig. 3). The most relevant recorded sequences occurred on February 1, 1988 with mainshock $M_D$ 4.1 and on February 14, 2002 with mainshock $M_D$ 4.9. The cumulative radiated seismic energy is located between a 2 and a 19 km depth with a peak at 13 km (Fig. 4). The fault plane solutions are mainly of thrust type with minor strike-slip events (Table 1). The most important damaging earthquakes in the past (Fig. 2) were the 1700 event ($I_0$ = VIII-IX, estimated magnitude 5.7), the 1788 event ($I_0$ = VIII-IX, estimated magnitude 5.6), the 1920 event ($I_0$ = VI-VII, estimated magnitude 5.3) and the 1928 event ($I_0$ = VIII-IX, estimated magnitude 5.7).

### *5.6. Belt 6*

The main tectonic structures are south-verging folds and thrusts, dipping at 40° to 60°. The deforming zone is characterized by a low-to-moderate seismic activity (Fig. 3), extending down to a 20 km depth, with maximum radiated seismic energy located at an 11 km depth (Fig. 4). The most important sequence recorded during the considered period followed the $M_D$ 4.1 event that occurred on May 28, 1998. Predominant thrust faulting is revealed by the fault plane solutions (Table 1). Minor normal and strike-slip events are also present. The most important earthquakes known from historical data (Fig. 2) were the 1794 event ($I_0$ = VII – VIII, estimated magnitude 5.4), the 1776 event ($I_0$ = VIII – IX, estimated magnitude 5.8) and the 1812 event ($I_0$ = VII – VIII, estimated magnitude 5.8).

### *5.7. Belt 7*

The tectonic style is characterized by dominant E-W oriented thrusts, north-dipping at 40° to 60°. The seismic activity is similar to that of Belt 6 (Fig. 3). The cumulative radiated seismic energy extends down to a 17 km depth with a maximum located at about an 11 km depth (Fig. 4). The most important recorded sequence that affected this zone during the examined period followed the $M_D$ 3.8 event that occurred on October 5, 1991. The focal mechanisms are mainly of thrust type (Table 1). In the past, this belt has been struck by severe earthquakes (Fig. 2) like the 1511 event ($I_0$ = IX, estimated magnitude 6.5) and the 1976 event ($I_0$ = IX – X, $M_L$ 6.4). The focal mechanisms of the 1976 major events, obtained by computing the centroid-moment tensor

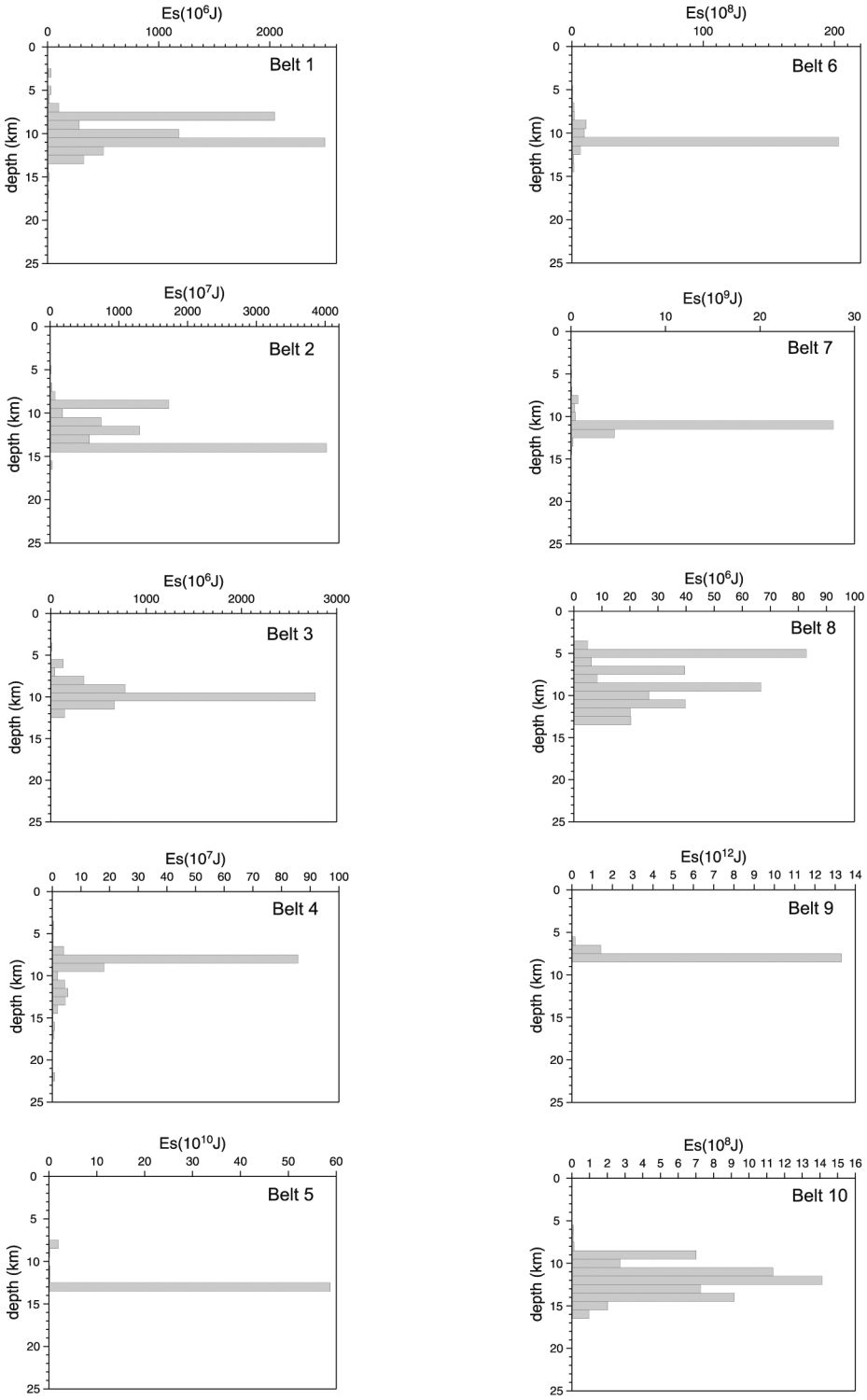


Fig. 4 - Depth distribution of the cumulative radiated seismic energy (in J) for each deforming belt.

(Pondrelli *et al.*, 2001), show fault plane orientations from about E-W to NE-SW, N-NW dipping, with strikes between 23° and 37°, consistent with the tectonic setting of the belt.

### *5.8. Belt 8*

The main tectonic lineament is the approximately E-W-oriented Fella-Sava Line. Its kinematic aspects are the same as Belt 4. Minor NW-SE oriented strike-slip faults are also present. A very low seismic activity is detected (Fig. 3), extending down to about a 14 km depth (Fig. 4). The maximum recorded duration magnitude in the considered period was 2.8. Thrust and normal focal mechanisms characterize this deforming belt (Table 1). No relevant shocks from historical data are known inside the belt.

### *5.9. Belt 9*

The dominant tectonic structure of the zone consists of a set of dextral strike-slip faults, about NW-SE oriented and minor NE-dipping thrusts (Bajc *et al.*, 2001). The belt is characterized by the highest seismic activity of the study area (Fig. 3). The thickness of the seismogenic layer is 16 km, with peaks of the radiated seismic energy recognizable at a 7-8 km depth (Fig. 4). The most important recorded seismic sequences, that occurred in 1998 (mainshock $M_D$ 5.6) and in 2004 (mainshock $M_D$ 5.1), are related to the NW-SE strike-slip faults. Strike slip and thrust fault plane solutions prevail (Table 1), with minor normal faulting events. No significant historic earthquakes are documented for this zone.

### *5.10. Belt 10*

The main tectonic lineaments are NW-SE oriented strike-slip faults and similarly oriented thrusts dipping 50°-60° to the NE. The seismic activity is low (Fig. 3) with maximum recorded $M_D$ 3.4. The radiated seismic energy extends down to about a 17 km depth, with maximum peaks located between 11 and 14 km down (Fig. 4). The focal mechanisms are of various types with a slight predominance of thrust faulting (Table 1). No relevant historic earthquakes are located inside this belt, even if the location of the 1511 event ($I_0$ = IX, estimated magnitude 6.5) is close to this area. It should be pointed out that the uncertainties of historical data do not allow a reliable location even if the damage seems mostly localized in Belt 7 (CPTI Working Group, 2004). The most important well documented shocks (Fig. 2) occurred in 1716 and in 1898 with $I_0$ = VII (estimated magnitude 4.8).

The choice of the deforming belts in some cases, could appear somehow subjective. The deforming belts 1, 2 and 3 in the western part of the study area are considered distinct because of noticeable differences in the tectonic pattern, seismic activity, focal mechanisms, Bouguer anomaly pattern. Belts 4 and 8 are characterized by different tectonic patterns. A particular case is represented by the adjoining deforming belts 5, 6 and 7 that seem to show common characteristics. The main reasons why we consider these deforming belts to be distinct are the following. The tectonic setting of Belt 5 (E-W oriented thrusts and backthrusts, vertical fault systems) is different from that of belts 6 and 7. Belt 5 is characterized by a different pattern of Bouguer anomalies and their horizontal gradient modulus (Gentile *et al.*, 2000). Furthermore, differences were found in the 3D Vp and Vp/Vs tomographic anomalies (Gentile *et al.*, 2000) and in the crustal pattern of elastic moduli (De Franco *et al.*, 2004). An apparent, stronger similarity seems to characterize the belts 6 and 7. However, Belt 7 is characterized by maximum

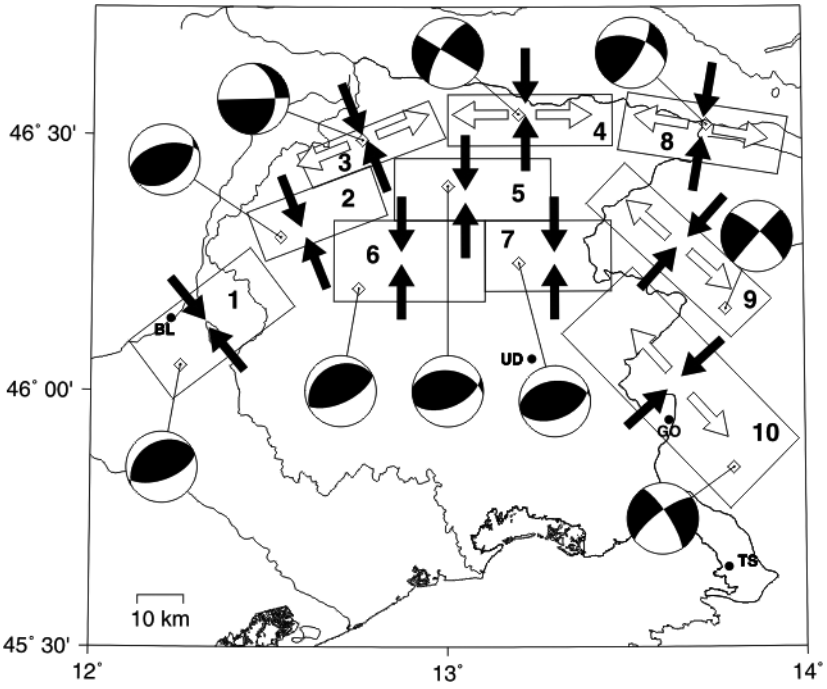


Fig. 5 - Deforming belts. Focal spheres represent the focal mechanism resulting from moment tensor summation. Black arrows indicate compression, white arrows indicate extension. Other symbols as in Fig. 1.

interference and overlapping of Alpine and Dinaric faults (Carulli and Ponton, 1988) and by more severe crustal shortening (Venturini and Carulli, 2002). Differences between the two deforming zones are also recognizable in the spatial pattern of the 3D Vp and Vp/Vs tomographic anomalies (Gentile *et al.*, 2000) and crustal elastic moduli (De Franco *et al.*, 2004). The pattern of the horizontal gradient modulus of the Bouguer anomalies (Gentile *et al.*, 2000) is different in the two zones. Finally, Gentile and Slejko (1990) considered two distinct seismogenic zones, corresponding approximately to belts 6 and 7, in their seismotectonic study of the central Friuli area. Deforming belts 9 and 10 are considered distinct, mainly for their differences in the tectonic pattern, seismic activity and focal mechanisms.

## 6. Results and discussion

The results of the present analysis for each deforming belt are summarized in Tables 2 and 3. The pattern of the seismic strain is shown in Fig. 5.

### *6.1. Belt 1*

The seismic moment release over 23 years is 3.3 x $10^{14}$ Nm. The resulting seismic deformation is compressional. The dominant components $\dot{\varepsilon}_{11}$ and $\dot{\varepsilon}_{33}$, are related to compression in the NW-SE direction and thickening of the seismogenic layer. The corresponding velocities are 3.9 x $10^{-4}$

Table 2 - Components of the strain rate tensor $\dot{\varepsilon}$. The column FS indicates the multiplication factor/year. Positive values indicate extension or thickening, negative values indicate compression or thinning.

| Belt | FS | $\dot{\varepsilon}_{11}$ | $\dot{\varepsilon}_{12}$ | $\dot{\varepsilon}_{13}$ | $\dot{\varepsilon}_{22}$ | $\dot{\varepsilon}_{23}$ | $\dot{\varepsilon}_{33}$ |
|---|---|---|---|---|---|---|---|
| 1 | 10-11/yr | -2.46 | -0.85 | 1.11 | 0.62 | 0.44 | 1.84 |
| 2 | 10-10/yr | -3.07 | 0.24 | -0.72 | 0.46 | -0.49 | 2.60 |
| 3 | 10-11/yr | -1.40 | 1.83 | -2.53 | 1.46 | -1.18 | -0.05 |
| 4 | 10-12/yr | -5.76 | 2.81 | 1.86 | 5.42 | 0.98 | 0.33 |
| 5 | 10-10/yr | -8.41 | 1.40 | 1.36 | 0.67 | -2.38 | 7.73 |
| 6 | 10-11/yr | -4.72 | 2.32 | 3.81 | -1.23 | -1.63 | 5.96 |
| 7 | 10-11/yr | -4.35 | 1.34 | 0.38 | 0.65 | -0.47 | 0.36 |
| 8 | 10-12/yr | -1.17 | 1.72 | 0.51 | 0.06 | -0.47 | 1.10 |
| 9 | 10-09/yr | -0.53 | 9.79 | 0.30 | 0.64 | -2.21 | -0.11 |
| 10 | 10-12/yr | -1.83 | 5.94 | 2.80 | 0.87 | -2.14 | 0.96 |

mm/year for the compression and 3.1 x $10^{-4}$ mm/year for the vertical extension.

### *6.2. Belt 2*

The seismic moment released in the examined period is 2.8 x $10^{15}$ Nm. The strain rate tensor shows predominance of compressional deformation. The dominant component $\dot{\varepsilon}_{11}$ takes place in a mean NNW-SSE direction at an average rate of 3.4 x $10^{-3}$ mm/year. The other dominant component $\dot{\varepsilon}_{33}$ is associated with thickening of the seismogenic layer at a rate of about 5.2 x $10^{-3}$ mm/year.

### *6.3. Belt 3*

The cumulative seismic moment release is 1.98 x $10^{14}$ Nm. The geometry of deformation is strike-slip with normal component. The $\dot{\varepsilon}_{12}$ component of the tensor strain rate is related to the dextral strike motion, with rate 3.3 x $10^{-4}$ mm/year. The $\dot{\varepsilon}_{22}$ component is related to an extension in the N50° direction and the $\dot{\varepsilon}_{11}$ component is characterized by a shortening along the N320° direction. The corresponding rates are 4.6 x $10^{-4}$ mm/year and 1.3 x $10^{-4}$ mm/year, respectively.

### *6.4. Belt 4*

The belt is characterized by strike-slip deformation with cumulative seismic moment 6.32 x $10^{13}$ Nm. The dominant components of the tensor strain rate are $\dot{\varepsilon}_{11}$ and $\dot{\varepsilon}_{22}$, corresponding to 0.6 x $10^{-4}$ mm/year of compression in the N-S direction and to 1.9 x $10^{-4}$ mm/year of extension in the E-W direction. The $\dot{\varepsilon}_{12}$ is related to a dextral strike-slip motion that takes place at 0.6 x $10^{-4}$ mm/year.

### *6.5. Belt 5*

The deformation pattern is mainly compressional, with a seismic moment released 1.1 x $10^{16}$ Nm. The compressional deformation takes place at 1.3 x $10^{-2}$ mm/year in the N-S direction. The other dominant component of the strain rate tensor is the thickening of the seismogenic layer occurring at about 1.4 x $10^{-2}$ mm/year. The contribution of the largest event of this area ($M_D$ 4.9)

Table 3 - Components of the velocity tensor V. All values are in mm/year. The column FV indicates the multiplicating factor. Positive values indicate extension or thickening, negative values indicate compression or thinning

| Belt | FV | $V_{11}$ | $V_{12}$ | $V_{13}$ | $V_{22}$ | $V_{23}$ | $V_{33}$ |
|---|---|---|---|---|---|---|---|
| 1 | 10-4 | -3.94 | - 2.74 | 3.77 | 2.08 | 1.51 | 3.13 |
| 2 | 10-3 | -3.37 | 0.54 | -2.90 | 1.41 | -1.98 | 5.21 |
| 3 | 10-4 | -1.26 | 3.30 | -7.08 | 4.60 | -3.33 | -0.08 |
| 4 | 10-4 | -0.66 | 0.64 | 0.63 | 1.92 | 0.33 | 0.05 |
| 5 | 10-2 | -1.31 | 0.43 | 0.51 | 0.25 | -0.90 | 1.46 |
| 6 | 10-3 | -0.59 | 0.58 | 1.52 | -0.41 | -0.65 | 1.19 |
| 7 | 10-3 | -0.67 | 0.41 | 0.13 | 0.18 | -0.16 | 0.62 |
| 8 | 10-5 | -1.52 | 4.47 | 1.44 | 0.23 | -1.33 | 1.54 |
| 9 | 10-2 | -0.66 | 24.48 | 0.98 | 2.81 | -7.07 | -0.18 |
| 10 | 10-4 | -0.38 | 2.49 | 0.95 | 0.46 | -0.73 | 0.16 |

is about 87% of the total sum of the seimic moment.

### *6.6. Belt 6*

The geometry of deformation is compressional. The total seismic moment released in the considered period is 8.4 x $10^{14}$ Nm. The dominant component of the tensor strain rate $\dot{\varepsilon}_{33}$ is associated with the thickening of the seismogenic layer at a rate of 1.2 x $10^{-3}$ mm/year. The other dominant component is $\dot{\varepsilon}_{11}$, corresponding to compression along a N-S direction at a rate of 0.6 x $10^{-3}$ mm/year. The component $\dot{\varepsilon}_{12}$ is related to a dextral motion occurring at about 0.6 x $10^{-3}$ mm/year.

### *6.7. Belt 7*

The belt is characterized by a compressional deformation with a smaller strike-slip component. The seismic moment release is 4.3 x $10^{14}$ Nm. The dominant components of the strain rate tensor are $\dot{\varepsilon}_{11}$ and $\dot{\varepsilon}_{12}$, which correspond to a 0.6 x $10^{-3}$ mm/year compression in the N-S direction and to a 0.4 x $10^{-3}$ mm/year dextral motion. The vertical extension takes place at 0.62 x $10^{-3}$ mm/year.

### *6.8. Belt 8*

The moment tensor summation shows that the deformation is accommodated by a prevailing strike-slip motion, with a total seismic moment released of 1.97 x $10^{13}$ Nm. The dominant component of the strain rate tensor is $\dot{\varepsilon}_{12}$ related to a shear dextral motion that takes place at about 4.5 x $10^{-5}$ mm/year. The $\dot{\varepsilon}_{11}$ component points to a compression in the NNE-SSW direction at a rate of 1.5 x $10^{-5}$ mm/year while the other dominant component $\dot{\varepsilon}_{33}$ shows thickening of the crust with a velocity of 1.5 x $10^{-5}$ mm/year.

### *6.9. Belt 9*

The summed moment tensor shows that the belt is subject to a strike-slip motion along an approximate N130°E direction, with a released seismic moment of 1.2 x $10^{17}$ Nm. The strain rate tensor shows that the deformation is mainly accommodated by a dextral strike-slip motion at a

rate of 0.24 mm/year. The $\dot{\varepsilon}_{22}$ component is related to an extension at rate of 2.8 x $10^{-2}$ mm/year and the component normal to the boundary $\dot{\varepsilon}_{11}$ reveals compression at a rate of 0.6 x $10^{-2}$ mm/year. The seismogenic layer is undergoing a thinning at about 0.2 x $10^{-2}$ mm/year. The most two severe shocks recorded by the OGS seismic network in the examined period (the 1998 $M_D$ 5.6 event and the 2004 $M_D$ 5.1 event), that account for about the 99% of the total released seismic moment, are located in this area.

*6.10. Belt 10*

The geometry of deformation of this belt is mainly strike-slip with a released seismic moment of 1.85 x $10^{14}$ Nm. The dominant component of the strain rate tensor is $\dot{\varepsilon}_{12}$, related to dextral strike-slip motion along about N 140°E at rate 2.5 x $10^{-4}$ mm/year. The compressive motion normal to the boundary of the belt takes place at about 0.4 x $10^{-4}$ mm/year. The seismogenic layer is undergoing to thickening with a rate of 1.6 x $10^{-5}$ mm/year.

The seismic strain pattern obtained from the moment tensor summation provides a complex picture of the active crustal deformations affecting the north-eastern part of the Adria microplate. This area is formed by several deforming belts, each with a peculiar seismicity pattern, tectonics and type of focal mechanisms.

To conclude, compressional deformation characterizes belts 1 and 2 in the western part of the study area (Fig. 5). The dominant components of the tensor strain rate are related to compression changing its strike from NW-SE (Belt 1) to NNW-SSE (Belt 2) and to the thickening of the seismogenic layer. The seismic deformation is higher in the case of Belt 2. The deformation velocities related to the compression are 3.4 x $10^{-3}$ mm/year (Belt 2) and 3.9 x $10^{-4}$ mm/year (Belt 1).

The calculated strain tensors indicate that the dominant mode of deformation of the northern belts 3, 4, 8 is dextral strike-slip motion (Fig. 5). The amount of seismic deformation and the resulting deformation rates are not homogeneous. The data examined in the period 1984-2006 evidence that Belt 3 is undergoing a major deformation. In particular, the rates of motion, corresponding to the component $\dot{\varepsilon}_{12}$ of the tensor strain rate, are 3.3 x $10^{-4}$ mm/year (Belt 3), 0.6 x $10^{-4}$ mm/year (Belt 4) and 4.5 x $10^{-5}$ mm/year (Belt 8). According to the calculated strain rate tensor, Belt 3 is affected by crustal thinning while belts 4 and 8 are characterized by crustal thickening. The seismic deformation of eastern belts 9 and 10 (Fig. 5), both characterized by Dinaric tectonics, is mainly accommodated by a dextral strike-slip motion, that takes place at a rate of 0.24 mm/year and 2.5 x $10^{-4}$ mm/year, respectively. Belt 9 is affected by the maximum amount of seismic deformation and strain rate in the study area. The vertical component of the strain rate tensor indicates crustal thinning in Belt 9 and crustal thickening in Belt 10.

The geometry of deformation of belts 5, 6 and 7 (Fig. 5), revealed by the tensor strain rate calculations shows common features. All zones, that are located in the central part of the study area, are undergoing to dominant compression in the N-S direction and a thickening of the seismogenic layer. The highest amount of seismic deformation and the highest deformation rate take place in Belt 5. Belts 6 and 7 are characterized by about the same magnitude of the component $\dot{\varepsilon}_{11}$ (N-S compression). The rate of thickening ($\dot{\varepsilon}_{33}$ component) of the seismogenic layer of Belt 6 is higher than that of Belt 7. The rates of motion associated with compressional

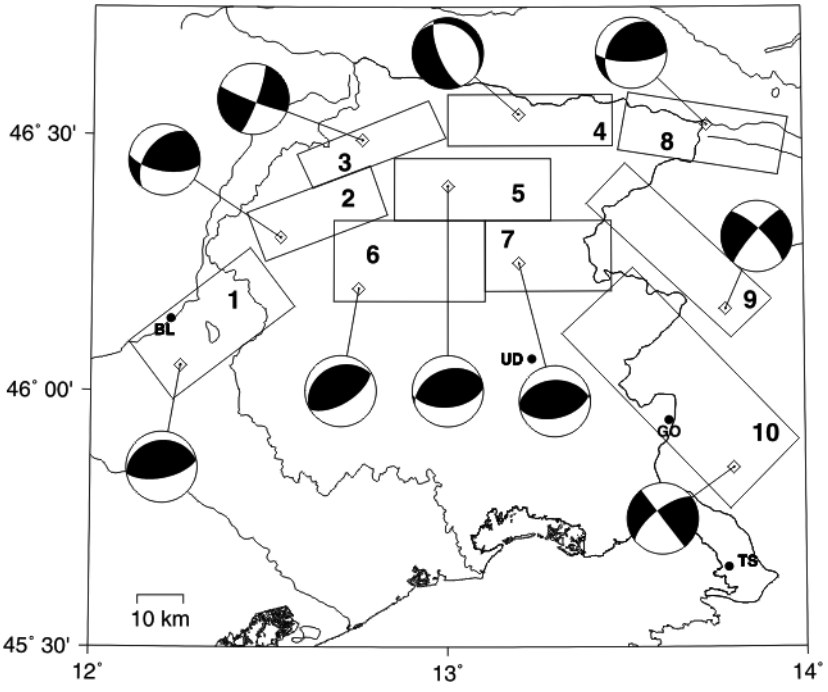


Fig. 6 - Deforming belts. Focal spheres represent the composite focal mechanism. Other symbols as in Fig. 1.

strain are 1.3 x $10^{-2}$ mm/year (Belt 5) and about 0.6 x $10^{-3}$ mm/year (Belts 6 and 7).

We compare composite focal mechanism solutions to those from moment tensor solutions. Composite focal mechanism solutions could help to provide a rough description of the stress regime in the deforming belts. Most of the focal mechanisms of the data set are related to small earthquakes, with $M_D \leq 3.5$ (Fig. 3) or ambient seismicity. So, the composite focal mechanisms can provide also insight into how small earthquakes are related to the seismic strain pattern calculated for deforming belts from moment tensor summation. Some deforming belts (3, 8 and 10 in Table 1) are characterized by a heterogeneous set of fault plane solutions without a prevailing focal mechanism. The composite focal mechanisms (Fig. 6) and the focal mechanisms resulting from moment tensor summation of the deforming belts 1, 5, 6, 7, 9 and 10 are identical. Fault plane solutions are similar for belts 2 and 3. The strike of the nodal planes varies slightly in Belt 2 and the amount of the strike-slip component of the cumulative focal mechanism is increased in the case of Belt 3. Major discrepancies are observed in the case of belts 4 and 8. The composite focal mechanism for Belt 4 is normal while that calculated from moment tensor summation is strike-slip. The deforming Belt 8 is characterized by a reverse, composite focal mechanism, with strike-slip component, in contrast with the strike-slip mechanism obtained by the moment tensor summation.

In short, the ambient seismicity reflects the seismic strain pattern calculated from the moment tensor summation except in the deforming belts 4 and 8. In these belts, the seismic strain calculated from the moment tensor summation is dominated by the major shocks and the focal

mechanisms could be too scarce for a reliable evaluation of the seismic strain pattern. However, the prevailing mode of seismic deformation is a dextral strike-slip motion, in accordance with the dominant tectonic movements (Venturini, 1991; Merlini *et al.*, 2002).

As pointed out above, the Friuli upper crust, imaged by tomographic inversion (Gentile *et al.*, 2000), is characterized by discontinuous blocks and wedges, marked by lateral heterogeneities in Vp and Vp/Vs values, interpreted as variations of the mechanical strength of rocks and/or degree of fracturing.

The heterogeneity plays a key role in determining the fracture patterns, fault initiation and development (Tang, 1997; Amitrano, 2006). So the wide variability of focal mechanisms of some deforming belts can be attributed to the mechanical heterogeneity of the crust and to the pre-existing faults. Most of the radiated seismic energy (Fig. 4) is caused by the largest earthquakes ($M_D > 3.5$) of the data set. Their fault plane solutions appear to be consistent with surface tectonic lineaments (Bressan *et al.*, 2003, 2007).

Grenerczy *et al.* (2005) calculated the velocity field in the northern Adriatic region from GPS station velocities. They estimated that the Adria-Alpine collision takes place at a rate of about 2.3 mm/year. The rates of motion of the deforming belts calculated from the moment tensor summation are considerably lower, suggesting that a significant part of the deformation occurs aseismically. We recall that the maximum coseismic rate is 0.24 mm/year associated to the dextral strike-slip motion of Belt 9, along a NW-SE direction. The rates of motion of the other deforming belts, related to the dominant mode of deformation range from $4.5 \times 10^{-5}$ mm/year (Belt 8) to $1.3 \times 10^{-2}$ mm/year (Belt 5).

The calculated strain rate tensors and the related velocities have to be examined taking into account the limits of the approach used in this investigation. The time interval considered (23 years) is probably too short to be considered representative of longer periods characterizing the seismic phenomena. Furthermore, the values of the strain rate tensor depend on the shape and the dimension of the boxes used to define the deforming seismogenic belts. Even if the deforming zones appear well constrained by the seismicity pattern, tectonics, focal mechanisms and geophysical data, their definition can be, to some extent, arbitrary.

## 7. Conclusions

The seismic deformation pattern provides a detailed picture of the kinematics of the northern margin of the Adria microplate and puts in evidence the dominant tectonic processes that accommodate its interaction with the Eurasian plate. Furthermore, the recognized spatial distribution of seismic strain can contribute to the definition of the spatial sampling and the resolution of the geodetic measurements for the comparison between geodetic and seismic strain.

The major seismogenic belts that are likely to generate most of the present day deformation in the Friuli-Venezia Giulia region and in western Slovenia, have been recognized on the basis of a seismicity pattern, tectonic style and focal mechanisms.

The seismic deformation and the deformation rates have been calculated from the moment tensor summation method, following the approach of Kostrov (1974) and Jackson and McKenzie (1988). A total of 279 focal mechanisms, in the period 1984-2006, were used. The geometry of deformation of the investigated area is not homogeneous, with a significant strain partitioning

among the deforming belts, being involved in the counterclockwise rotation of the Adriatic microplate.

The dominant mode of deformation of belts 1 and 2, located in the western part of the study area, is compressional, switching its orientation from NW-SE to NNW-SSE direction, with corresponding velocities 3.9 x $10^{-4}$ mm/year (Belt 1) and 3.4 x $10^{-3}$ mm/year (Belt 2).

The prevailing mode of deformation in the northern and western belts (3, 4, 8, 9 and 10) is related to a dextral strike-slip motion. The calculated strain rate tensors show variations in the amount of seismic deformation and the resulting deformation rates. In particular, Belt 9 is characterized by the maximum amount of seismic deformation and strain rate in the study area, with an estimated deformation velocity of 0.24 mm/year. The rates related to a dextral strike-slip motion of the other belts vary from 4.5 x $10^{-5}$ mm/year to 3.3 x $10^{-4}$ mm/year.

A N-S compressional deformation is dominant in belts 5, 6 and 7, located in the central part of the study area, with the major amount of seimic deformation affecting Belt 5. The velocity of deformation related to compressional strain varies from 0.6 x $10^{-3}$ mm/year (Belt 7) to 1.3 x $10^{-2}$ mm/year (Belt 5).

The vertical component of the strain rate tensors indicates that the deforming belts are undergoing to crustal thickening excepting belts 3 and 9, affected by crustal thinning.

The rates of motion of the deforming belts, compared with the Adria-Alpine rate collision, calculated from GPS station velocities, suggest that a significant part of the deformation occurs aseismically.

**Acknowledgments**. The local seismic network is managed by the Dipartimento Centro di Ricerche Sismologiche of the Istituto Nazionale di Oceanografia e Geofisica Sperimentale (OGS) with the financial contribution of the Regione Friuli-Venezia Giulia. We thank M. Zivcic for kindly providing data of Slovenian seismicity. Thanks are due also to S. Urban for help in the graphics and to the technical staff for data acquisition.

## REFERENCES

Amitrano D.; 2006: *Failure by damage accumulation in rocks*. Int. J. Fract., **193**, 369-381.

Anderson H. and Jackson J.; 1987: *Active tectonics of the Adriatic Region.* Geophys. J.R. Astr. Soc., **91**, 937-983.

Bajc J., Aoudia A., Saraò A. and Suhadolc P.; 2001: *The 1998 Bovec-Krn mountain (Slovenia) earthquake.* Geophys. Res. Lett., **28**, 1839-1842.

Barbano M.S.; 1990: *Revisione di alcuni terremoti dell'Italia nord-orientale nella prima metà del XX secolo.* In: Atti Conv. GNDT, Linea di Ricerca 1, Zonazione sismica e Riclassificazione sismica, Pisa, 25-27 giugno 1990, **2**, pp. 223-246.

Barbano M.S.; 1993: *Reassessing intensity of some Friuli earthquakes at the turn of the eighteenth century.* Terra Nova, **5,** 467-474.

Barbano M.S., Kind R. and Zonno G.; 1985: *Focal parameters of some Friuli earthquakes (1976-1979) using complete theoretical seismograms.* J. Geophys., **58**, 175-182.

Bernardis G., Poli M.E., Renner G., Snidarcig A. and Zanferrari A.; 1996: *Le tre sequenze sismiche del 1996 a Claut (Prealpi Carniche).* In: Atti del 15° convegno Gruppo Nazionale di Geofisica della Terra Solida, Esagrafica,

Roma, Italy, 11-13 novembre, pp. 343-348.

Bressan G., Bragato P.L. and Venturini C.; 2003: *Stress and strain tensors based on focal mechanisms in the seismotectonic framework of the Eastern Southern Alps*. Bull. Seism. Soc. Am., **93**, 1280-1297.

Bressan G., Kravanja S. and Franceschina G.; 2007: *Source parameters and stress release of seismic sequences occurred in the Friuli-Venezia Giulia region (Northeastern Italy) and in Western Slovenia.* Phys. Earth Planet. Int., **160**, 192-214.

Camassi R. and Stucchi M.; 1997: *NT4.1. Un catalogo parametrico di terremoti di area italiana al di sopra della soglia del danno*. GNDT, Milano, 95 pp.

Carulli G.B. and Ponton M.; 1988: *Interpretazione strutturale profonda della Alpi Carniche centrali.* Rend. Soc. Geol. It., **11**, 251-252.

Carulli G.B. and Ponton M.; 1992: *Interpretazione strutturale profonda del settore centrale carnico-friulano.* Studi Geologici Camerti, CROP1-1A, **2**, 275-284.

Cassano E., Maino A., Amadei G., Cesi C., Salvadei R., Ventura R., Visicchio F., Zanoletti F., Paulucci G. and Todisco A.; 1989: *Carta gravimetrica d'Italia scala 1:100000.* Servizio Geologico, Istituto Poligrafico e Zecca dello Stato, Roma.

Castellarin A.; 1979: *Il problema dei raccorciamenti crostali nel Sudalpino.* Rend. Soc. Geol. Ital., **1**, 21-23.

Castellarin A., Cantelli L., Fesce A.M., Mercier J.L., Picotti V., Pini G.A., Prosser G. and Selli L.; 1992: *Alpine compressional tectonics in the Southern Alps. Relationship with the N-Apennines,* Annales Tectonicae, **VI**, 62-94.

CPTI Working Group; 2004: *Catalogo Parametrico dei Terremoti Italiani, vers. 2004 (CPTI04).* Bologna, INGV, http://emidius.mi.ingv.it.

De Franco R., Bressan G. and Gentile G.F.; 2004: *Elastic moduli and seismogenic aspects of the Friuli upper crust.*. Boll. Geof. Teor. Appl., **45**, 71-87.

Franceschina G., Kravanja S. and Bressan G.; 2006: *Source parameters and scaling relationships in the Friuli-Venezia Giulia (Northeastern Italy) region.* Phys. Earth Planet. Int., **154**, 148-167.

Galadini F., Poli M.E. and Zanferrari A.; 2005: *Seismogenic sources potentially responsible for earthquakes with M≥6 in the eastern Southern Alps (Thiene-Udine sector, NE Italy).* Geophys. J. Int., **161**, 739-762.

Gentile G.F. and Slejko D.; 1990: *A 3D study of the fault pattern in Friuli (northeastern Italy) from focal mechanism intensity.* Boll. Geof. Teor. Appl., **32**, 199-214.

Gentile G.F., Bressan G., Burlini L. and De Franco R.; 2000: *Three-dimensional Vp and Vp/Vs models of the upper crust in the Friuli area (northeastern Italy).* Geophys. J. Int., **141**, 457-478.

Grenerczy G., Sella G., Stein S. and Kenyeres A.; 2005: *Tectonic implications of the GPS velocity field in the northern Adriatic region.* Geophys. Res. Lett., **32**, L16311, doi:10.1029/2005GL022947.

Jackson J. and McKenzie D.; 1988: *The relationship between plate motions and seismic moment tensors, and the rates of active deformation in the Mediterranean and Middle east.* Geophys. J., **93**, 45-73.

Kostrov B.V.; 1974: *Seismic moment and energy of earthquakes and seismic flow of rocks.* Izv. Acad. Sci. USSR Phys. Solid Earth, Engl. Transl., **1**, 23-44.

Lee W.H.K. and Lahr J.C.; 1975: *HYPO71 (revised): a computer program for determining hypocenter, magnitude and first motion pattern of local earthquakes.* U.S. Geol. Surv., Open File Rep. 75-311 Menlo Park, 113 pp.

Mantovani E., Albarello D., Tamburelli C. and Babbucci D.; 1996: *Evolution of the Tyrrhenian basin and surrounding regions as a result of the Africa-Eurasia convergence.* J. Geodynamics, **21**, 35-72.

Merlini S., Doglioni C., Fantoni R. and Ponton M.; 2002: *Analisi strutturale lungo un profilo geologico tra la linea Fella-Sava e l'avampaese adriatico (Friuli Venezia Giulia – Italia)*. Mem. Soc. Geol. It., **57**, 293-300.

Nocquet J.M. and Calais E.; 2003: *Crustal velocity field of western Europe from permanent GPS array solutions, 1996-2001*. Geophys. J. Int., **154**, 72-88.

Papazachos C.B. and Kiratzi A.; 1992: *A formulation for reliable estimation of active crustal deformation and its application to central Greece.* Geophys. J. Int., **111**, 424-432.

Poli M.E., Peruzza L., Rebez A., Renner G., Slejko D. and Zanferrari A.; 2002: *New seismotectonic evidence from the analysis of the 1976-1977 and 1977-1999 seismicity in Friuli (NE Italy).* Boll. Geof. Teor. Appl., **43**, 53-78.

Poli M.E. and Renner G.; 2004: *Normal focal mechanisms in the Julian Alps and Prealps: seismotectonic implications*

*for the Italian-Slovenian border region.* Boll. Geof. Teor. Appl., **45**, 51-69.

Pondrelli S.; 1999: *Pattern of seismic deformation in the Western Mediterranean*. Ann. Geof., **42**, 57-70.

Pondrelli S., Morelli A. and Boschi E.; 1995: *Seismic deformation in the mediterranean area estimated by moment tensor summation.* Geophys. J. Int., **122**, 938-952.

Pondrelli S., Ekström G. and Morelli A.; 2001: *Seismotectonic re-evaluation of the 1976 Friuli, Italy, seismic sequence*. J. of Seism., **5**, 73-83.

Rebez A. and Renner G.; 1991: *Duration magnitude for the northeastern Italy seismometric network.* Boll. Geof. Teor. Appl., **33**, 177-186.

Scarascia S. and Cassinis R.; 1997: *Crustal structures in the central-eastern Alpine sector: a revision of the available DSS data.* Tectonophysics, **271**, 157-188.

Sirovich L. and Pettenati F.; 2004: S*ource inversion of intensity patterns of earthquakes: a destructive shock in 1936 in northeast Italy*. Journ. Geophys. Res., **109**, B10309, doi: 10.1029/2003JB002919.

Slejko D., Carulli G.B., Nicolich R., Rebez A., Zanferrari A., Cavallin A., Doglioni C., Carraro F., Castaldini D., Iliceto V., Semenza E. and Zanolla C.; 1989: *Seismotectonics of the Eastern Southern-Alps: a review.* Boll. Geof. Teor. Appl. **31**, 109-136.

Tang C.; 1997: *Numerical simulation of progressive rock failure and associated seismicity*. Int. J. Rock Mech. Sci., **34**, 249-261.

Vai G.B., Venturini C., Carulli G.B. and Zanferrari A.; 2002: *Alpi e Prealpi Carniche e Giulie. Guide Geologiche Regionali.* Società Geologica Italiana, Roma, 389 pp.

Venturini C.; 1991: *Cinematica neogenico-quaternaria del Sudalpino orientale (settore friulano).* Studi Geol. Camerti, Vol. Spec., 109-116.

Venturini C. and Carulli G.B.; 2002: *Nealpine structural evolution of the carnic Alps central core (Mt. Amariana, Mt. Plauris, Mt. San Simeone).* Mem. Soc. Geol. It., **57,** 273-281.

Ward S.N.; 1994: *Constraints on the seismotectonics of the central Mediterranean from very long baseline interferometry.* Geophys. J. Int., **117**, 441-452.

Whitcomb J.H.; 1973: *Part I. A study of the velocity structure of the Earth by the use of core phases. Part II. The 1971 San Fernando earthquake series, focal mechanisms and tectonics*, Ph.D. Thesis, California Institute of Technology, Pasadena, 443 pp.

Wyss M., Liang B., Tanigawa W.R. and Wu X.; 1992: *Comparison of stress and strain tensors based on fault plane solutions in Kaoiki, Haway.* J. Geophys. Res., **97**, 4769-4790.

Zoback M.L.; 1992: *First- and second-order patterns of stress in the lithosphere: the world stress map project.* J. Geophys. Res., **97**, 11703-11728.

*Corresponding author:* Gianni Bressan
Istituto Nazionale di Oceanografia e di Geofisica Sperimentale
Dipartimento Centro Ricerche Sismologiche
Via Treviso 55, 33100 Cussignacco, Udine (Italy)
phone: +39 0432 522422; fax: +39 0432 522474; e-mail: gbressan@inogs.it